https://doi.org/10.20965/jrm.2023.p0417

Paper:

Aerodynamic Drag of a Tilt-Rotor UAV During Forward Flight in Rotary-Wing Mode

Takateru Urakubo*, Koki Wada*, Kohtaro Sabe, Shinji Hirai**, and Masafumi Miwa*****

*Kobe University
1-1 Rokkodai-cho, Nada-ku, Kobe 657-8501, Japan
E-mail: t.urakubo@silver.kobe-u.ac.jp
**Aerosense Inc.
5-41-10 Koishikawa, Bunkyo-ku, Tokyo 112-0002, Japan
E-mail: {kohtaro.sabe, shinji.hirai}@aerosense.co.jp
***Tokushima University
2-1 Minamijosanjima-cho, Tokushima 770-8506, Japan
E-mail: miw@tokushima-u.ac.jp
[Received October 28, 2022; accepted December 15, 2022]

This paper examines the aerodynamic drag force acting on a tilt-rotor UAV that has three mini fans and a main rotor with a tilt mechanism. The mini fans are embedded in the nose and the left and right wings. The main rotor is located near the center of the vehicle, and its front half is surrounded by the trailing edge of the nose in rotary-wing mode. The downward airflow from the fans and the main rotor generates an aerodynamic drag force called momentum drag, which is linearly proportional to the airspeed of UAV. To verify the existence of momentum drag, parameter identification of drag coefficients is performed from experimental data where the UAV flies forward in rotary-wing mode. The drag force is also investigated using computational fluid dynamics simulations. These experimental and numerical results are consistent with theoretical results based on momentum theory.

Keywords: VTOL, parameter identification, CFD, momentum drag

1. Introduction

Vertical take-off and landing (VTOL) aircraft can switch its flight mode between rotary-wing mode and fixed-wing mode. In the rotary-wing mode, it can hover, take off, and land vertically like a helicopter. In the fixed-wing mode, it can fly fast with high energy efficiency like an airplane. VTOL unmanned aerial vehicles (UAVs) are expected to perform many tasks such as surveillance, monitoring, transportation and delivery, in a wider range and at a higher speed than multicopter UAVs [1].

Many configurations of VTOL UAVs such as tilt-rotor and tilt-wing types have been proposed and developed using multiple propulsors driven by electric motors [2–4]. We have been developing an electric VTOL UAV since 2015. The flight mode can be switched by tilting the main rotor that is located near the center of the body. Three mini fans are equipped in the nose and the left and right wings to enable attitude control of the UAV. The main rotor and three mini fans provide the lift force in rotary-wing mode as multiple lift fans installed in the UAV.

The aerodynamic force applied to VTOL aircraft with lift fans has been an interesting research topic, because of the complex interaction between propulsion and aerodynamics [5, 6]. The flow fields in hover and transition highly depend on the airframe, fan wake, crosswind, and so on [7]. The lift force generated by fans can be reduced when the aircraft is close to the ground. The airflow induced by the fan wake can slightly reduce the lift force, even without the ground effect [8]. In particular, the drag force can become much larger in a crossflow owing to the effect of *momentum drag* [9, 10]. The fan streams cause a drag force that is linearly proportional to airspeed.

In order to control the flight of VTOL UAVs as fully as possible, it is necessary to understand their aerodynamic characteristics sufficiently [11–14]. In particular, from a practical perspective, it is desirable to achieve a backward transition from fixed-wing mode to rotary-wing mode quickly and accurately to avoid wasting energy and time [15]. The aerodynamic drag during the transition should be revealed to stop the UAVs just above the target point from the high-speed cruise, as illustrated in **Fig. 1**. In a low-speed flight near the end of backward transition, the momentum drag would be applied to VTOL UAVs with lift fans. The design of a controller for low-speed flight requires the modeling of the drag force.

In this paper, we examine the aerodynamic drag applied to a prototype VTOL UAV during low-speed forward flight in rotary-wing mode, through parameter identification from experimental data and computational fluid dynamics (CFD) analysis (**Fig. 1**). Based on a longitudinal model of the UAV, the aerodynamic coefficients for drag are estimated by applying the least-squares method to experimental flight data. The estimation results indicate that the momentum drag is applied to the UAV. We

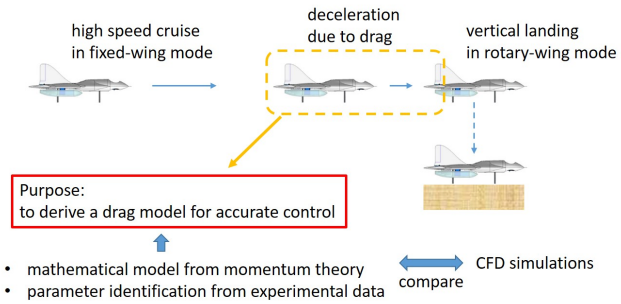

Fig. 1. Motivation and approach to derive a drag model.

Fig. 2. First prototype of a tilt-rotor UAV (wingspan: 2.2 m).

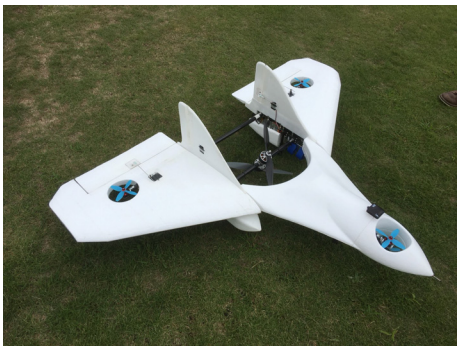

Fig. 3. Second prototype of a tilt-rotor UAV (wingspan: 1.43 m).

also perform CFD simulations for the UAV to verify their correspondence with the experimental results. Finally, we discuss these results by comparing with the theoretical results in [9]. The main contribution of this paper is to demonstrate the existence of momentum drag for the VTOL UAV in rotary-wing mode based on experimental flight data as well as numerical and theoretical analyses.

2. Tilt-Rotor UAV

Two prototypes of tilt-rotor UAVs developed since 2015 are shown in **Figs. 2** and **3**. The wingspan and length of the first prototype in **Fig. 2** are respectively 2.2 m and 1.6 m and its total weight is about 8.2 kg. The second prototype shown in **Fig. 3** was developed by Aerosense Inc. in 2016, and is smaller than the first prototype. The wingspan and length are respectively 1.43 m and 1.08 m, and the total weight is approximately 5.74 kg. The maximum operating times of these prototypes are about 25 and 15 min, respectively, and the cruising speed is about 70 km/h for both prototypes. They are expected to be primarily used for monitoring and inspection tasks.

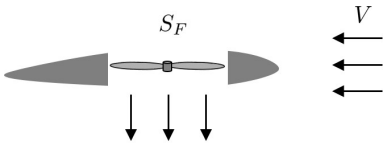

Fig. 4. Fan-in-wing in a crosswind.

For both prototypes, a pair of coaxial rotors with a tilt mechanism is mounted at the center of the airframe, and generates mainly the force to lift and propel the vehicle. To stabilize the attitude in hover, three fans are installed at the front nose and the left and right wings. The fan at the front nose is also a pair of coaxial rotors for the second prototype, and the two fans at the left and right wings rotate in opposite directions to cancel their counter torques. All the rotors and fans are driven by electric brushless motors. The UAV also has four control surfaces installed in the main and vertical wings to stabilize the attitude in fixed-wing mode. Two control surfaces located at the trailing edges of main wings can be deflected independently to function as elevons. The other two control surfaces in the vertical wings operate as rudders by deflecting synchronously. For this configuration of the VTOL UAV, the blades of rotors and fans are not exposed outside the UAV. This is a desirable feature of the configuration, because blades rotating at high speeds are dangerous for people close to the UAV.

In this study, we focus on the second prototype in **Fig. 3** to examine the aerodynamic drag acting on it, particularly for forward flight in rotary-wing mode. It should be noted that momentum drag, which will be described in the next section, may be applied to the UAV, because the main rotor and three mini fans are surrounded by the airframe.

3. Longitudinal Model for Drag Investigation

3.1. Momentum Drag for Fan-in-Wing

In this subsection, the momentum drag for fan-in-wing aircraft that was shown in [9] will be briefly summarized for later use in dynamic model derivation. When a fan-in-wing is located in a crosswind V as shown in **Fig. 4**, the air velocity from the fan is aligned with the fan shaft owing to the duct of the fan. Then, from the momentum conservation, the following drag force D_m is generated:

$$D_m = n\rho S_F V_J V = \sqrt{n\rho S_F T_S} V \quad \cdots\cdots (1)$$

where V is the airspeed of aircraft, ρ is the air density, S_F is the fan area, and T_S is the static thrust generated by the fan. V_J is the fan-exit velocity in hover with static thrust T_S, and is represented as

$$V_J = \sqrt{\frac{T_S}{n\rho S_F}} \quad \cdots\cdots\cdots\cdots (2)$$

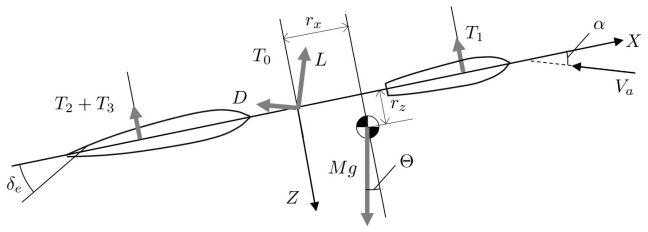

Fig. 5. Longitudinal model of the UAV.

The parameter n denotes the ratio of the induced velocity in the far wake to that at the fan, and is assumed to be 1 [9]. Note that, although the momentum drag depends on the angle of attack α in [9], it can be approximated for a small α using Eq. (1).

For the VTOL UAV shown in Section 2, three mini fans are embedded into the front nose and the left and right wings, and the main rotor is also surrounded by the airframe like a fan-in-wing. Momentum drags can be caused at these four thrusters for the UAV.

3.2. Longitudinal Dynamic Model

In this subsection, we summarize the equations of translational motion in rotary-wing mode where the thrust force of the main rotor is tilted along the upward direction of the body. Assuming that the lateral velocity, roll angle, roll rate, and yaw rate are all zero, the longitudinal model of the UAV will be derived below.

A body coordinate frame is introduced such that the X- and Z-axes are along the forward and downward directions of the body, respectively, and the origin is located at the tilt axis of the main rotor (**Fig. 5**). Using the body coordinate frame, the longitudinal equations of translational motion are represented as follows:

$$M\begin{bmatrix} \dot{U}+QW+r_z\dot{Q}-r_xQ^2 \\ \dot{W}-QU-r_x\dot{Q}-r_zQ^2 \end{bmatrix} = Mg\begin{bmatrix} -\sin\Theta \\ \cos\Theta \end{bmatrix}+\begin{bmatrix} X_t \\ Z_t \end{bmatrix}+\begin{bmatrix} X_a \\ Z_a \end{bmatrix} \quad \ldots (3)$$

where the translational velocity of the UAV is denoted by $[U,W]$ in the body coordinate frame, Θ is the pitch angle, and Q is the pitch rate. The mass of the UAV is denoted as M, $[r_x,r_y]$ is the position vector of the mass center, and g is the gravitational acceleration. The equation of rotational motion about the pitch axis is omitted because it is not used in this paper.

The translational forces caused by the rotor thrusts along the X- and Z-axes are denoted as X_t and Z_t, respectively. In the rotary-wing mode with zero tilt angle, they are represented as follows:

$$X_t = 0 \quad \ldots (4)$$

$$Z_t = -(T_0+T_1+T_2+T_3) \quad \ldots (5)$$

where T_0 is the thrust force of main rotor, and T_1, T_2 and T_3 are the thrust forces of mini fans in the nose and the left and right wings, respectively. Since the main rotor and the nose fan are coaxial rotors composed of upper and lower rotors, T_0 and T_1 represent the sum of thrust forces caused by the upper and lower rotors.

The aerodynamic forces acting on the UAV are denoted by X_a and Z_a in Eq. (3), and can be expressed as follows:

$$X_a = L\sin\alpha - D\cos\alpha \quad \ldots (6)$$

$$Z_a = -L\cos\alpha - D\sin\alpha \quad \ldots (7)$$

where L and D are lift and drag forces acting on the UAV, and α is the angle of attack. Assuming that a constant wind $-V_w$ exists along the X-axis, α is represented as

$$\alpha = \tan^{-1}\left(\frac{W}{U+V_w}\right) \quad \ldots (8)$$

Note that the elevon angle δ_e is set to be zero throughout this paper, because we focus on the momentum drag in rotary-wing mode.

3.3. Drag Force Representation

From Eqs. (3), (6), and (7), the drag force D can be expressed in the following form:

$$\begin{aligned} D &= -X_a\cos\alpha - Z_a\sin\alpha \\ &= f_D(U,W,\dot{U},\dot{W},\Theta,Q,\dot{Q},T_a,V_w) \end{aligned} \quad \ldots (9)$$

where $T_a = \sum_{i=0}^{3} T_i$. It should be noted that, in flight experiments, all the arguments of f_D can be obtained from the measurement data; that is, the drag force can be estimated from the data.

On the other hand, the following model is commonly used for the drag force of fixed-wing aircraft [16].

$$D_c = \frac{1}{2}\rho V_a^2 S C_D \quad \ldots (10)$$

$$C_D = C_{D_0} + C_{D_\alpha}\alpha + C_{D_q}\frac{c}{2V_a}Q \quad \ldots (11)$$

where S is the wing area, and c is the mean aerodynamic chord. The airspeed V_a is expressed as follows:

$$V_a = \sqrt{(U+V_w)^2+W^2} \quad \ldots (12)$$

For the VTOL UAV in **Fig. 3**, the momentum drag described in Section 3.1 would be caused at the main rotor and three mini fans as follows:

$$D_m = \sqrt{\rho}V_a\sum_{i=0}^{3}\sqrt{n_iS_iT_i} \quad \ldots (13)$$

where the quantities with respect to the main rotor, nose fan, left-wing fan, and right-wing fan are expressed with subscripts 0, 1, 2, and 3, respectively. Note that, although the main rotor and the nose fan are composed of coaxial rotors, Eq. (1) holds for them based on momentum theory. In Eq. (13), S_0 and S_1 denote the disc area of upper or lower rotor for the main rotor and the nose fan, respectively, and n_0 and n_1 represent the ratio of the induced velocity in the far wake to that at the lower rotor.

Since the areas of the three fans are identical, we denote them as S_f. For hover flight in rotary-wing mode, the thrust force of main rotor T_0 is set to be $0.7Mg$, and

the total thrust force of three mini fans $T_1+T_2+T_3$ is set to be $0.3Mg$. In the flight experiments for forward flight in rotary-wing mode, their average values approximately satisfy these values, although the thrust forces fluctuate owing to altitude and attitude control. Then, by substituting $n_i \approx 1$, $S_1 = S_2 = S_3 = S_f$, $T_0 \approx 0.7Mg$ and $T_1+T_2+T_3 \approx 0.3Mg$ into Eq. (13), the momentum drag can be rewritten as

$$D_m \approx \sqrt{\rho Mg}\left(\sqrt{0.3S_f}+\sqrt{0.7S_0}\right)V_a \equiv k_D V_a \quad . \quad (14)$$

By adding the momentum drag in Eq. (14) to the commonly used model in Eq. (10), we represent the drag force as follows:

$$D = D_c + D_m = \frac{1}{2}\rho V_a^2 S C_D + k_D V_a = \frac{1}{2}\rho V_a^2 S C_D' \quad (15)$$

where

$$C_D' = C_{D_0} + C_{D_\alpha}\alpha + C_{D_q}\frac{c}{2V_a}Q + \frac{2k_D}{\rho S V_a} \quad . \quad . \quad . \quad . \quad (16)$$

4. Aerodynamic Drag Analysis

In this section, we examine the aerodynamic drag acting on the VTOL UAV during forward flight in rotary-wing mode using two approaches: parameter identification from flight data and CFD analysis.

4.1. Parameter Identification from Flight Data

From Eqs. (9) and (15), we obtain

$$f_D(U,W,\dot{U},\dot{W},\Theta,Q,\dot{Q},T_a,V_w) = \frac{1}{2}\rho V_a^2 S\left(C_{D_0}+C_{D_\alpha}\alpha+C_{D_q}\frac{c}{2V_a}Q+\frac{2k_D}{\rho S V_a}\right) \quad (17)$$

In the above equation, C_{D_0}, C_{D_α}, C_{D_q} and k_D are unknown parameters, and the other variables and parameters are obtained from flight data and UAV dimensions. Eq. (17) can be rewritten as follows:

$$\frac{2f_D}{\rho V_a^2 S} = C_D' = \boldsymbol{X}\boldsymbol{\theta} \quad . \quad . \quad . \quad . \quad . \quad . \quad . \quad . \quad . \quad . \quad (18)$$

where

$$\boldsymbol{X} = \left[1, \alpha, \frac{c}{2V_a}Q, \frac{2}{\rho S V_a}\right] \quad . \quad . \quad . \quad . \quad . \quad . \quad . \quad . \quad . \quad (19)$$

$$\boldsymbol{\theta} = [C_{D_0}, C_{D_\alpha}, C_{D_q}, k_D]^{\mathrm{T}} \quad . \quad . \quad . \quad . \quad . \quad . \quad . \quad . \quad . \quad (20)$$

To identify the parameters $\boldsymbol{\theta}$, we gathered flight data by performing several manual flights. The experimental flights consisted of the following flight patterns:

- Forward flights at various speeds with different pitch angles.
- Forward flights with periodic variations in pitch angle and speed.

From the flight data, the unknown parameters $\boldsymbol{\theta}$ were estimated using the equation-error method [17]. Before applying the least-squares method to the data, a low-pass filter was used to remove high-frequency noise. The cut-off frequency was chosen as 10 Hz considering the sampling frequency of 50 Hz and the natural frequencies of a linearized model for longitudinal motion. From Eq. (18), we obtain the following linear equations:

$$\boldsymbol{z} = \tilde{\boldsymbol{X}}\boldsymbol{\theta} + \boldsymbol{\nu} \quad . \quad . \quad . \quad . \quad . \quad . \quad . \quad . \quad . \quad . \quad . \quad . \quad . \quad (21)$$

$$\boldsymbol{z} = [C_D'(1), C_D'(2), \ldots, C_D'(N)]^{\mathrm{T}} \quad . \quad . \quad . \quad . \quad . \quad . \quad (22)$$

$$\tilde{\boldsymbol{X}} = [\boldsymbol{X}(1)^{\mathrm{T}}, \boldsymbol{X}(2)^{\mathrm{T}}, \ldots, \boldsymbol{X}(N)^{\mathrm{T}}]^{\mathrm{T}} \quad . \quad . \quad . \quad . \quad . \quad . \quad (23)$$

where N is the number of data points, and $\boldsymbol{z}$ and $\tilde{\boldsymbol{X}}$ are calculated from the data smoothed by the low-pass filter. By minimizing the errors $\boldsymbol{\nu}$, we obtain the estimated value of $\boldsymbol{\theta}$ as follows:

$$\hat{\boldsymbol{\theta}} = (\tilde{\boldsymbol{X}}^{\mathrm{T}}\tilde{\boldsymbol{X}})^{-1}\tilde{\boldsymbol{X}}^{\mathrm{T}}\boldsymbol{z} \quad . \quad . \quad . \quad . \quad . \quad . \quad . \quad . \quad . \quad . \quad . \quad (24)$$

The values of $\hat{\boldsymbol{\theta}}$ estimated from the flight data, where $N = 1969$, are summarized in **Table 1**. To calculate $\boldsymbol{z}$ and $\tilde{\boldsymbol{X}}$ in Eq. (24), we obtained the values of U, W, $\dot{U}$, $\dot{W}$, Θ, Q, and $\dot{Q}$ from the measurement data by the onboard autopilot (Pixhawk, 3D Robotics). The thrust forces T_0, T_1, T_2, and T_3 were estimated from the results of preliminary experiments that examined the relationship between throttle commands and static thrusts for each rotor. To compensate for variations in thrust due to temperature and battery conditions, we modified the relationship based on the actual throttle commands during hover in each manual flight. The wind speed V_w was obtained for each flight by roughly averaging the measurements from a wind speed sensor that was located at the flight test site. The area S and the chord c were set to be 0.538 m^2 and 0.431 m, respectively.

Table 1. Estimated values of drag parameters.

Parameter	Value
C_{D_0}	-0.217
C_{D_α} [1/rad]	-0.236
C_{D_q} [1/rad]	-3.32
k_D [Ns/m]	2.70

Figure 6 shows the drag coefficient C_D' calculated based on the flight data in three different ways. The blue dots represent the values of $\boldsymbol{z}$, which were obtained by calculating f_D from the flight data. The orange dots denote the values of $\tilde{\boldsymbol{X}}\hat{\boldsymbol{\theta}}$ that are the values of C_D' expected from the identified parameters $\hat{\boldsymbol{\theta}}$. To verify the effects of introducing the momentum drag D_m, we also performed parameter identification when the drag force D is modeled as $D = D_c$ without D_m. The values of $\tilde{\boldsymbol{X}}[\hat{C}_{D_0}, \hat{C}_{D_\alpha}, \hat{C}_{D_q}]^{\mathrm{T}}$ obtained in this case are represented by the green dots in **Fig. 6**. From the blue dots, C_D' appears to be in inverse proportion to V_a, and the orange dots obtained from the model with D_m also reflect this trend. However, the green dots obtained from the model without D_m could not duplicate this trend. The root mean squared error in parameter

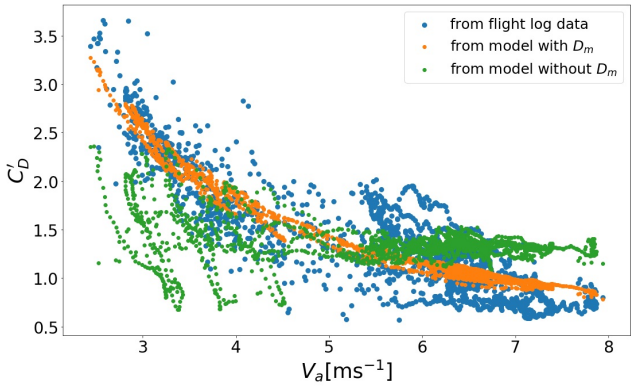

Fig. 6. Drag coefficient C'_D calculated from flight data, model with D_m and model without D_m.

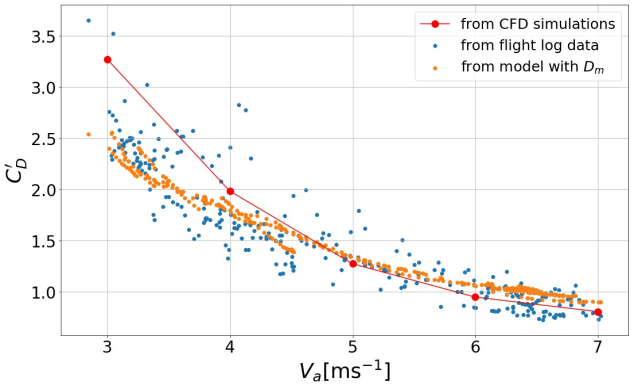

Fig. 8. Drag coefficient C'_D obtained from CFD simulations.

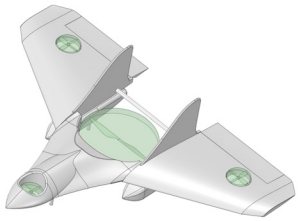

Fig. 7. UAV model for CFD simulations.

identification, that is, $\sqrt{\|\boldsymbol{\nu}\|^2/N}$, is 0.26 for the model with D_m and 0.53 for the model without D_m. These results would indicate that the momentum drag D_m should be included in the aerodynamic model of the VTOL UAV.

4.2. CFD Simulations

To verify the results obtained from the parameter identification in Section 4.1, we performed CFD simulations using ANSYS Fluent. **Fig. 7** shows the UAV model used for the simulations, where rotating zones for rotors are placed as painted in green by exploiting the multiple reference frame (MRF) approach [18]. Although the main rotor and the nose fan consist of coaxial rotors, each is modeled as a single rotor for simplicity. The rotation speed of each rotor was chosen such that the thrust force generated from each rotor in CFD approximately coincided with that during hover in the experiments. The computational domain was set to be at least four times larger than the wing span and the height of the UAV, so that the flow around the UAV would not be affected by the domain boundary. The domain was divided into about 26 million cells, with a boundary layer mesh on the UAV surface where the first layer height was 2.5×10^{-5} m, the growth rate was 1.2, and the maximum number of layers was 10. Assuming the flow to be steady and incompressible without heat transfer, we used the SIMPLE algorithm for iterative calculations and the SST $k-\omega$ model to deal with turbulence [19]. The air density and viscosity were set as 1.225 kg/m^3 and 1.789×10^{-5} kg/ms, respectively.

With the above settings, CFD simulations were performed for $V_a = 3,4,5,6$ and 7 m/s at $\alpha = 0°$ to examine the variation in the drag force D due to the airspeed V_a. The drag coefficients C'_D obtained by CFD simulations are shown by the red dots in **Fig. 8**. The CFD results also show that C'_D is inversely proportional to V_a, that is, the momentum drag exists. In the figure, the values of C'_D obtained from the flight data and the model with D_m are also represented by the blue and orange dots. Only the points that satisfy $|\alpha| \leq 5°$ are drawn for comparison with the CFD results obtained at $\alpha = 0°$.

5. Discussion

From **Fig. 8**, both the parameter identification and CFD analysis indicate that C'_D is inversely proportional to V_a. These results are consistent with the mathematical model shown in Eq. (14). Since $S_0 = 0.0856$ m^2, $S_f = 0.00811$ m^2, and $M = 5.74$ kg for the UAV in **Fig. 3**, the value of k_D can be calculated from Eq. (14) as $k_D = 2.60$ Ns/m assuming that $\rho = 1.225$ kg/m^3 and $g = 9.807$ m/s^2. This theoretical value is close to that obtained from the parameter identification in **Table 1**.

However, the values of C'_D obtained by CFD analysis are larger than those represented by the orange dots, for $V_a = 3$ and 4 m/s. One possible reason for this is that the actual drag force cannot be accurately represented at all speeds using Eq. (15). For the UAV shown in **Fig. 3**, the airframe surrounds only the front half of the main rotor. Owing to this asymmetric geometry, a non-zero drag force might be caused like the wall effect even when $V_a = 0$ m/s, which would increase C'_D significantly at low speeds. However, it should be noted that, even for a large difference in C'_D at $V_a = 3$ m/s, the difference in drag force is not very large because V_a is small. Although the difference in C'_D results in a model error when constructing a system model using the drag model (15), the model error is much smaller than that with the drag model (10), and would be easily compensated by a controller.

To reveal the aerodynamic forces of the UAV in more detail, more extensive CFD simulations and wind tunnel tests would be required. Note that the wind disturbances tend to cause larger errors in C'_D at lower speeds in the

outdoor experiments. The disturbances make an accurate parameter identification difficult at lower speeds, and also demand a feedback control for stabilization. Although a smaller model error is generally desirable for control, the system model with the drag model (15) developed in this paper may be sufficient for controller design. Controller design and performance evaluation using the drag model (15) will be necessary in the future.

The drag force model obtained in this paper would be utilized for motion planning and control of the UAV, even though it is an approximation of the drag as mentioned above. For example, a quick and accurate back-transition from fixed-wing mode to rotary-wing mode is desirable for VTOL UAVs from the perspectives of battery consumption and flight time [15]. The deceleration near rotary-wing mode can be predicted more accurately by considering the momentum drag revealed in this paper. As another example, the model can be used to analyze the wind speed conditions under which the UAV can hover with limited thrust force.

Moreover, parameter identification can be performed to examine the lift force and pitch moment of the UAV in a similar manner. However, the results should be checked and interpreted more carefully, because the variation and error in the estimated thrust force of each rotor would substantially affect the identification results. Inaccurate thrust estimation makes it difficult to obtain accurate models of aerodynamic lift force and pitch moment. From a control perspective, the total lift force and total pitch moment applied to the UAV can be directly manipulated through the rotor thrusts, and the altitude and pitch angle would be successfully controlled even without accurate models of aerodynamic lift force and pitch moment. Because there is no thrust force that directly propels the UAV forward and backward in the rotary-wing mode, the analysis of the drag force would be more significant for motion planning and control.

There are many types of VTOL UAVs other than the UAV shown in **Fig. 3**. Since the aerodynamic forces are highly dependent on the configuration of UAV such as tilt angles and location of rotors, it would be necessary to examine the forces for each UAV in a similar manner as in this paper. The results in this paper indicate that momentum drag should be considered when developing the aerodynamic model if the UAV has lift fans surrounded by an airframe.

6. Conclusion

In this paper, we examined the aerodynamic drag of a tilt-rotor UAV by using parameter identification and CFD simulations. The experimental and numerical results indicate that the UAV is subjected to the momentum drag that is linearly proportional to the airspeed, and are also consistent with the conventional mathematical model. The obtained drag model could be utilized for motion planning and control of the UAV near its rotary-wing mode.

Acknowledgments

This work was partially supported by the Kawanishi Memorial ShinMaywa Education Foundation.

References:

[1] K. Nonami, "Drone technology, cutting-edge drone business, and future prospects," J. Robot. Mechatron., Vol.28, No.3, pp. 262-272, 2016.

[2] A. S. Saeed, A. B. Younes, S. Islam, J. Dias, L. Seneviratne, and G. Cai, "A review on the platform design, dynamic modeling and control of hybrid UAVs," Proc. of 2015 Int. Conf. on Unmanned Aircraft Systems, pp. 806-815, 2015.

[3] D. F. Finger, C. Braun, and C. Bil, "A review of configuration design for distributed propulsion transitioning VTOL aircraft," Proc. of the 2017 Asia-Pacific Int. Symposium on Aerospace Technology, pp. 1782-1796, 2017.

[4] P. M. Rothharr, P. C. Murphy, B. J. Bacon, I. M. Gregory, J. A. Grauer, R. C. Busan, and M. A. Croom, "NASA Langley distributed propulsion VTOL tilt-wing aircraft testing, modeling, simulation, control, and flight test development," Proc. of 14th AIAA Aviation Technology, Integration, and Operations Conf., AIAA 2014-2999, 2014.

[5] B. W. McCormick, Jr., "Aerodynamics of V/STOL flight," Dover, 1999.

[6] N. Thouault et al., "Experimental investigation of the aerodynamic characteristics of generic fan-in-wing configurations," The Aeronautical J., Vol.113, No.1139, pp. 9-20, 2009.

[7] R. E. Kuhn, R. J. Margason, and P. Curtis, "Jet induced effects: the aerodynamics of jet and fan powered V/STOL aircraft in hover and transition," Progress in Astronautics and Aeronautics, Vol.217, AIAA, 2006.

[8] A. J. Saddington and K. Knowles, "A review of out-of-ground-effect propulsion-induced interference on STOVL aircraft," Progress in Aerospace Sciences, Vol.41, Issues 3-4, pp. 175-191, 2005.

[9] H. H. Heyson, "Theoretical and experimental investigation of the performance of a fan-in-wing VTOL configuration," NASA TN D-7498, 1973.

[10] M. S. Selig, "Modeling propeller aerodynamics and slipstream effects on small UAVs in realtime," Proc. of AIAA Atmospheric Flight Mechanics 2010 Conf., AIAA 2010-7938, 2010.

[11] D. Rohr, M. Studiger, T. Stastny, N. R. J. Lawrance, and R. Siegwart, "Nonlinear model predictive velocity control of a VTOL tiltwing UAV," IEEE Robotics and Automation Letters, Vol.6, No.3, pp. 5776-5783, 2021. https://doi.org/10.1109/LRA.2021.3084888

[12] B. Li, J. Sun, W. Zhou, C.-Y. Wen, K. H. Low, and C.-K. Chen, "Transition optimization for a VTOL tail-sitter UAV," IEEE/ASME Trans. on Mechatronics, Vol.25, No.5, pp. 2534-2545, 2020. https://doi.org/10.1109/TMECH.2020.2983255

[13] J. B. Willis and R. W. Beard, "Pitch and thrust allocation for full-flight-regime control of winged eVTOL UAVs," IEEE Control Systems Letters, Vol.6, pp. 1058-1063, 2022.

[14] K. Kita, A. Konno, and M. Uchiyama, "Hovering control of a tail-sitter VTOL aerial robot," J. Robot. Mechatron., Vol.21, No.2, pp. 277-283, 2009.

[15] C. Kikumoto, T. Urakubo, K. Sabe, and Y. Hazama, "Back-transition control with large deceleration for a dual propulsion VTOL UAV based on its maneuverability," IEEE Robotics and Automation Letters, Vol.7, No.4, pp. 11697-11704, 2022.

[16] R. W. Beard and T. W. McLain, "Small unmanned aircraft: theory and practice," Princeton University Press, 2012.

[17] E. A. Morelli, "Practical aspects of the equation-error method for aircraft parameter estimation," Proc. of AIAA Atmospheric Flight Mechanics Conf. and Exhibit, AIAA 2006-6144, 2006.

[18] G. V. Shankaran and M. B. Dogruoz, "Validation of an advanced fan model with multiple reference frame approach," Proc. of 2010 12th IEEE Intersociety Conf. on Thermal and Thermomechanical Phenomena in Electronic Systems, 2010.

[19] H. K. Versteeg and W. Malalasekera, "An introduction to computational fluid dynamics," 2nd ed., Pearson Education Limited, Harlow, 2007.

Name:
Takateru Urakubo

ORCID:
0000-0002-7676-0204

Affiliation:
Associate Professor, Department of Information Science, Graduate School of System Informatics, Kobe University

Address:
1-1 Rokkodai-cho, Nada-ku, Kobe 657-8501, Japan

Brief Biographical History:
2001-2016 Assistant Professor, Kobe University
2007-2009 Visiting Research Scientist, Carnegie Mellon University
2016- Associate Professor, Kobe University

Membership in Academic Societies:
- Institute of Electrical and Electronics Engineers (IEEE)
- The Society of Instrument and Control Engineers (SICE)
- The Robotics Society of Japan (RSJ)
- The Institute of Systems, Control and Information Engineers (ISCIE)
- The Japan Society of Mechanical Engineers (JSME)
- The Japan Society for Aeronautical and Space Sciences (JSASS)

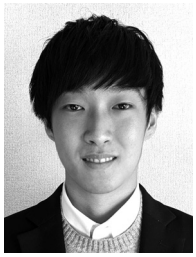

Name:
Koki Wada

Affiliation:
Department of Information Science, Graduate School of System Informatics, Kobe University

Address:
1-1 Rokkodai-cho, Nada-ku, Kobe 657-8501, Japan

Brief Biographical History:
2020- Department of Information Science, Graduate School of System Informatics, Kobe University

Name:
Kohtaro Sabe

ORCID:
0000-0003-0925-8211

Affiliation:
President and CEO, Aerosense Inc.

Address:
5-41-10 Koishikawa, Bunkyo-ku, Tokyo 112-0002, Japan

Brief Biographical History:
1996 Joined Sony Corporation
2012- Chief Distinguished Researcher, Business Design & Innovation Laboratory, Sony Corporation
2015 Founded Aerosense Inc.

Main Works:
- "Obstacle Avoidance and Path Planning for Humanoid Robots using Stereo Vision," Proc. of Int. Conf. on Robotics and Automation, 2004.
- "Self-regulation mechanism for continual autonomous learning in open-ended environments," Proc. of Epigenetic Robotics, 2009.

Name:
Shinji Hirai

Affiliation:
Aerosense Inc.

Address:
5-41-10 Koishikawa, Bunkyo-ku, Tokyo 112-0002, Japan

Brief Biographical History:
1982 Joined Sony Corporation
2017 Joined Aerosense Inc.

Main Works:
- VTOL and multicopter airframes development

Name:
Masafumi Miwa

Affiliation:
Associate Professor, Graduate School of Technology, Industrial and Social Science, Tokushima University

Address:
2-1 Minamijosanjima-cho, Tokushima 770-8506, Japan

Brief Biographical History:
1996- Assistant Professor, Faculty of System Engineering, Wakayama University
2007- Associate Professor, Institute of Technology and Science, Tokushima University
2016- Associate Professor, Graduate School of Science and Technology, Tokushima University
2017- Associate Professor, Graduate School of Technology, Industrial and Social Sciences, Tokushima University

Main Works:
- "Arbitrary Attitude Hovering Control of Quad Tilt Rotor Helicopter," J. Robot. Mechatron., Vol.28, No.3, pp. 328-333, 2016.

Membership in Academic Societies:
- The Japan Society of Mechanical Engineering (JSME)
- The Society of Instrument and Control Engineering (SICE)
- The Japanese Society of Experimental Mechanics (JSEM)